Supporting Methods

Simulations

Simulations were performed using custom written C++ software. Discrete time steps of 1 μs were used, during which single molecules would diffuse, fluoresce and undergo FRET. Unless stated otherwise, the diffusion coefficient was $D = 3*10^8$ nm^2 s^{-1}, and the extinction coefficient of each fluorophore was 10^5 M^{-1} cm^{-1}. The confocal spot was modeled with an incident laser intensity of 10^3 W cm^{-2} at its center, and decaying as a 3D Gaussian with radial width w_o = 500 nm, and axial width z_o= 1.5 μm.

PDA fitting

After calculating the shot-noise limited FRET distribution $P(E^*)$, it was fit to the observed distribution using a simple golden section method (31) to minimize the reduced chi-squared test statistic χ_r^2 (23):

$$\chi_r^2 = \frac{1}{z-y}\sum_{i=1}^{z}\frac{\left[Freq(X_i) - Freq_M(X_i)\right]^2}{Freq(X_i)} \qquad (1)$$

where y is the number of floating model parameters, z is the number of non-zero bins, and $Freq(X_i)$ and $Freq_M(X_i)$ represent the frequency of data falling into bin i in either the data or prediction, respectively. $\chi_r^2 = 1$ indicates a perfect fit, while $\chi_r^2 > 2$ generally indicates a poor fit.

Klenow Fragment (KF) of DNA polymerase I

The preparation of doubly labeled exo- KF has been described (8, 34). KF was labeled at positions 550 and 744 with ATTO647N and Cy3B respectively. The specificity of the labeling orientation was ≈88%; the extent of labeling was ≥ 70%. Labeled KF was a donation from Cathy M. Joyce and Olga Potapova.

DNA

Amino-modified oligonucleotides (IBA, G□ttingen, Germany) were labeled using NHS-conjugated fluorophores (Cy3B-NHS from GEHealthCare, Little Chalfont, UK, and Atto647N-NHS from ATTO-TEC, Siegen, Germany) according to the manufacturers' instructions. Oligos for double-stranded DNAs were purified on a reverse-phase column (μRPC C2/C18, GE Healthcare), while oligos for DNA hairpins were purified via denaturing PAGE. For DNA sequences, see Supporting Material Fig. S1.

Supporting Material Text

PDA implementation details

The expected $P(E^*)$ distribution excluding background was given in Eq. 3. Background in solutions containing no significantly fluorescent contaminants is due primarily to Raman scattering of the laser off of water molecules in the confocal volume; it is therefore poisson-distributed in time and independent of emission from the fluorescent particle. Incorporating background, the $P(E^*)$ distribution is:

$$P(E^*) = \sum_{all\ F_A, B_D, B_A\ yielding\ E^*} P\left(F_A \mid \langle E^* \rangle, F\right) \times P(F,T) \times P\left(B_D \mid T, r_D\right) \times P\left(B_A \mid T, r_A\right) \qquad \text{(S1)}$$

$$P\left(B_\gamma \mid T, r_\gamma\right) = \frac{\left(r_\gamma T\right)^{B_\gamma} e^{-\left(r_\gamma T\right)}}{B_\gamma !} \qquad \text{(S2)}$$

where $P\left(B_\gamma\right)$ is the distributions of background photons per burst in the γ-emission channel, r_γ are mean background rates, T is the duration of the burst and $P(F,T)$ is the joint distribution of fluorescence photons and burst durations (we use the joint distribution because F and T are dependent variables (1)).

In practice, the distribution of fluorescence photons $P(F)$ is unknown, but can be approximated from the experimental distribution of total photons, $P(N)$, via simple subtraction (2):

$$P(E^*) = \sum_{all\ F_A, B_D, B_A\ yielding\ E^*} \begin{aligned} &P\left(F_A \mid \langle E^* \rangle, N - B_A - B_D\right) \times P\left(N - B_A - B_D, T\right) \times \\ &P\left(B_D \mid T, r_D\right) \times P\left(B_A \mid T, r_A\right) \end{aligned} \qquad \text{(S3)}$$

This method is a simple approximation of the true $P(F)$ distribution; a more accurate deconvolution procedure has been described elsewhere (3).

PDA with static heterogeneity

PDA can be generalized in two ways: it can be extended to predict the shot-noise limited distribution for multiple molecules with different FRET values (static heterogeneity), or for a single molecule with multiple interconverting FRET states (dynamic heterogeneity). To account for static heterogeneity, Eq. 3 can be generalized to account for k species, where the j^{th} species has concentration c_j and fluorescence intensity distribution $P_j(F)$:

$$P(E^*) = \sum_{all\ F_A, B_D, B_A\ yielding\ E^*} \sum_{j=1}^{k} \left[c_j P\left(F_A \mid \langle E \rangle, F\right) \times P_j(F) \right] \times P\left(B_D\right) \times P\left(B_A\right) \qquad \text{(S4)}$$

This method requires "brightness correction" to calculate the distributions $P_j(F)$ from the overall $P(F)$, a process described in detail in (4); in our work, we use Eq. S4 only in cases of equally bright fluorescent species, allowing us to avoid the brightness-correction step and assume that all $P_j(F) = P(F)$. We note that a very useful extension of this method is model-independent extraction of the maximum-likelihood distribution of $\langle E^* \rangle$ from a given distribution $P(E^*)$, which we do not employ in the current work, but has been described in previous publications (3, 5).

PDA with dynamic heterogeneity

To account for dynamic heterogeneity, we recently generalized the PDA method to incorporate the existence of m dynamically-interconverting states i with mean proximity ratios $\langle E_i^* \rangle$ (6). The proximity ratio for each burst is calculated on the basis of fluorescence photons emitted in each state i, f_i, and the subset of those photons emitted in the acceptor channel, a_i:

$$E^* = \frac{B_A + \sum a_i}{B_D + B_A + \sum f_i} = \frac{B_A + \sum a_i}{N} \tag{S5}$$

where the acceptor photon counts a_i follow a binomial distribution with respect to f_i and E_i, as in Eq. 4. The FRET for each burst depends on the burst duration T, and on the distribution of times it spends in each state, $P(\vec{\tau} \mid T)$, which we determine using a Monte Carlo approach to simulate kinetic transitions. We assume uniform illumination intensity throughout the burst, such that the distribution of f_i is multinomial with residence times τ_i:

$$P(f_i \mid F, \vec{\tau}, \vec{b}) = (F!)\left[\prod_{i=1}^{m}\left(\frac{\left(b_i\tau_i / \sum(b_i\tau_i)\right)^{f_i}}{f_i!}\right)\right] \tag{S6}$$

where $F = \sum f_i$ and b_i is the brightness of molecule i. The overall distribution of FRET values is then:

$$P(E^*) = \sum_{all\left(B_A + \sum a_i\right)/N = E^*}\left[\prod_{i=1}^{m} P(a_i \mid f_i, \langle E_i^* \rangle) \times P(f_i \mid F, \vec{\tau}, \vec{b})\right] \times P(\vec{\tau} \mid T) \times P(F, T) \times P(B_D \mid T, r_D) \times P(B_A \mid T, r_A) \tag{S7}$$

This method is described in detail in (6).

Arrival-time PDA

In the dynamic PDA method, we use a Monte Carlo approach to simulate switching among FRET states for each burst, and therefore determine the distribution of times the molecule spends in each state, $P(\vec{\tau})$. We then determine the distribution of photons among different states, $P(\vec{f})$, by assuming uniform excitation intensity, such that $P(\vec{f})$ is multinomial with respect to $P(\vec{\tau})$, Eq. S6.

To improve the accuracy of our method, and preserve arrival time information for analysis with BVA, we eliminated the uniform-intensity assumption (or any other focal volume geometry assumption) for determining $P(\vec{f})$. We did this by incorporating $P(\vec{t})$, the distribution of experimental photon arrival times within the burst. Instead of determining $P(\vec{f} \mid \vec{\tau})$ using a uniform-intensity assumption, we determine $P(\vec{f} \mid \vec{t})$ by running our Monte-Carlo state-switching algorithm on a given burst, and simply counting the number of experimental photon arrival times occurring within each simulated state *i* (Fig. S9). Whereas the uniform intensity assumption assumes a uniform arrival-time distribution over time, the updated method draws from the experimental arrival-time distribution, eliminating the need for any assumptions about focal volume geometry and improving the accuracy of dynamic PDA predictions (Fig. S2). This is similar to the "recoloring" method recently used by Gopich and Szabo (7). The predicted *E** distribution using this method is:

$$P(E^*) = \sum_{all\left(B_A + \sum a_i\right)/N = E^*} \left[\prod_{i=1}^{m} P(a_i \mid f_i, \langle E_i^* \rangle) \right] \times P(\vec{f} \mid \vec{t}) \times P(F, T, \vec{t}) \times P(B_D \mid T, r_D) \times P(B_A \mid T, r_A) \qquad \text{(S8)}$$

We note that this approach is valid as long as all states in the experimental sample have similar photon arrival time distributions. This is because the true state from which an experimentally observed photon arises is unknown; however, when our Monte Carlo approach simulates state-switching, photons are assigned to a state regardless of their origin (Fig. S9). If the two states had significantly different distributions (e.g. due to very different brightnesses), these distributions would be averaged in our PDA predictions, and could produce inaccurate results.

Analytical method of obtaining confidence intervals

In the main text we proposed a Monte Carlo method of calculating accurate confidence intervals on σ_{E^*}. For Gaussian distributions of ε_{ij} with standard deviation σ_{E^*}, however (Eq. 5), the sampling distribution of standard deviations of the FRET has an analytical solution (8):

$$P(\sigma) = \frac{2\left(\frac{M}{2\sigma_{E^*}^2}\right)^{(M-1)/2} e^{-M\sigma^2/\left(2\sigma_{E^*}^2\right)} \sigma^{M-2}}{\Gamma\left((M-1)/2\right)} \qquad \text{(S9)}$$

where Γ is the gamma function: $\Gamma(z) = \int_0^\infty t^{z-1} e^{-t} dt$. Because the F_A giving rise to ε_{ij} is binomially distributed, the Gaussian assumption is valid for large n.

Bonferroni correction for multiple-hypothesis testing

When determining the confidence intervals for BVA, we employ a Bonferroni correction for multiple hypothesis testing (9), such that for the desired confidence interval $CI = 100\%(1-\alpha)$ with significance level α, we adjust the significance level to α / R, where R is the number of bins tested. This is because, as we test for dynamics in $R = 20$ separate bins, we effectively test each data set for the presence of dynamics 20 times. The Bonferroni correction simply avoids the increase in false positive rate this would cause if no correction were implemented. The Bonferroni-corrected upper-tail confidence interval $s_{E^*}^{CI}$ is defined according to $(1-\alpha/R) = \int_0^{s_{E^*}^{CI}} P_{MC}(\sigma)\, d\sigma$.

Window size in BVA

The impact of photon window size, *n*, on the detection of dynamics is small near the diffusion timescale (Fig. S4), though smaller windows are less computationally expensive to work with; unless otherwise indicated, we therefore set $n = 5$ throughout the text and in supplemental figures.

BVA accurately predicts the s_{E^*} of static FRET pairs

To test the ability of BVA to accurately predict the standard deviation, s_{E^*}, of molecules with static FRET, we simulated a series of molecules with different underlying FRET efficiencies ($\langle E^* \rangle = 0.2,\ 0.5,\ 0.8$). We first used Photon Distribution Analysis (PDA) to confirm that the E^* distributions were shot-noise limited, and therefore exhibited no detectable static or dynamic heterogeneity (Fig. S5, *A*; all χ_r^2 close to 1). We then used BVA to calculate the s_{E^*} over all E^* for these perfectly static FRET standards (Fig. S5, *B*, *triangles*), as well as a strict, 99.9% upper confidence interval, $s_{E^*}^{CI}$ (data below the confidence interval fall in the *gray region*). In all cases, the measured s_{E^*} fell below the confidence interval, showing good agreement with the hypothesis that no within-burst dynamics were present.

BVA shows no dynamics in a donor-only DNA control

Donor-only DNA's are an important control in ensuring that a given optical setup is not introducing artifactual dynamics into PDA analyses (2, 10). As such dynamics could in principle give rise to a dynamic signal by BVA, we analyzed a donor-only DNA sample to ensure this was not the case. The donor-only control is a double-stranded DNA labeled with only a donor fluorophore (Fig. S1, *A*); it therefore has no FRET, but $\langle E^* \rangle \approx 0.15$ due to leakage of donor emission into the acceptor channel (11). This leakage is unaffected by any dynamic heterogeneity in the DNA itself (assuming the DNA does not cause diffusion-timescale dynamic changes in the donor emission spectrum), but is sensitive to spatial mismatches in the detection efficiencies of the donor- and acceptor-emission detectors. We therefore characterized the donor-only control by PDA and BVA, to ensure our optical setup does not introduce apparent dynamics into otherwise-static samples when analyzed with

smFRET. We analyzed the donor-only control with both PDA and BVA; as expected, it exhibited a shot noise-limited $E*$ distribution ($\langle E* \rangle = 0.151 \pm .002$, $\chi_r^2 = 1.34$), and all s_{E*} values fell well within the 99.9% confidence interval (Fig. S10). Dynamics detected in our experiments on static and dynamic hairpin DNA's are therefore not due to optical artifacts.

Supporting Figures

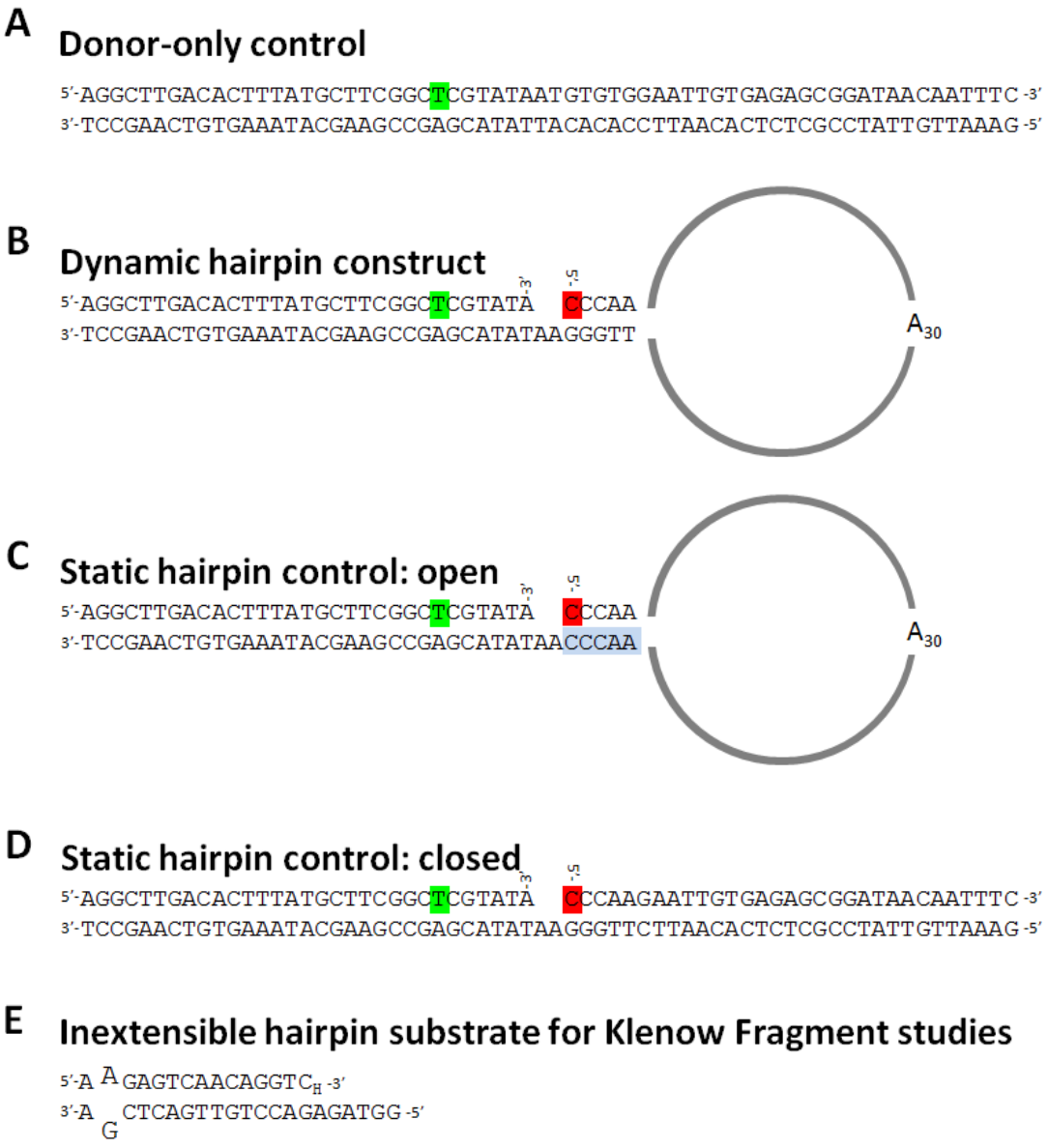

Figure S1. DNA and hairpin design. The nucleotides highlighted in green and red were labeled with Cy3B (donor) and Atto647N (acceptor) fluorophores respectively. All DNAs were PAGE-purified before analysis. (*A*) Donor-only-labeled DNA. (*B*) The hairpin construct is composed of a 31-nucleotide double-stranded region, a two-nucleotide single-stranded gap, another 5-nucleotide double-stranded region and a 30-adenine single stranded loop. The hairpin fluctuates dynamically due to spontaneous melting and re-annealing of the 5-nucleotide double stranded region. (*C*) As a control for the open (melted) form of the hairpin, we constructed a similar hairpin with a mismatch in the 5-nucleotide double-stranded region (*highlighted in blue*). (*D*) As a static control for the closed (annealed) form of the hairpin, we replaced the 30-adenine loop with a 26-basepair double-stranded region. (*E*) Hairpin template-primer used in Klenow Fragment studies. The 3' terminus contains a dideoxynucleotide to prevent successful nucleotide incorporation.

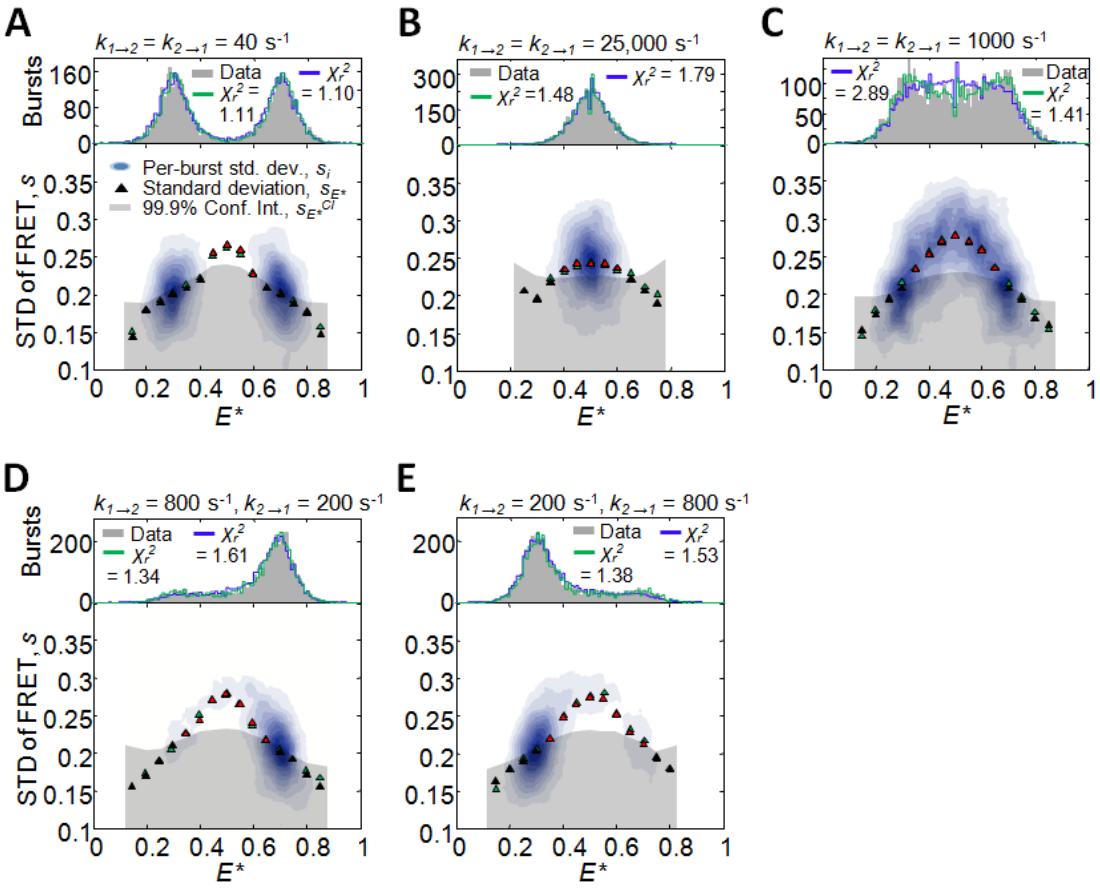

Figure S2. BVA of PDA predictions can accurately predict the s_{E^*} profile of simulated molecules. We simulated a series of molecules undergoing dynamic changes in FRET between $\langle E_1^* \rangle = 0.3$ and $\langle E_1^* \rangle = 0.7$ with equal forward and reverse rates of (*A*) 40 s^{-1}, (*B*) 1000 s^{-1} and (*C*) 25,000 s^{-1}, with forward and reverse rates of 800 s^{-1} and 200 s^{-1} respectively (*D),* or with forward and reverse rates of 200 s^{-1} and 800 s^{-1} respectively (*E*) . In all cases, PDA was used to predict the shot-noise limited histogram expected for each species (using the given parameters). BVA was then run on both the simulated data (s_{E^*}, *black and red triangles*), and the PDA-predicted data, (s_{E^*}, *green triangles*), and compared. Qualitatively, the two sets of triangles (and therefore s_{E^*} values) matched up very well, with no apparent systematic deviations. For comparative purposes, we also plotted PDA predictions (*A–E*, *blue lines*) using our original dynamic PDA method (6), which assumes a uniform excitation intensity and does not preserve photon arrival-time data (and therefore cannot be analyzed by BVA; see Supporting Material Text). In general, the "arrival-time PDA" method we use in this work (*green lines*) outperforms the original PDA method (*blue lines*) in accurately recapitulating the *E** histogram.

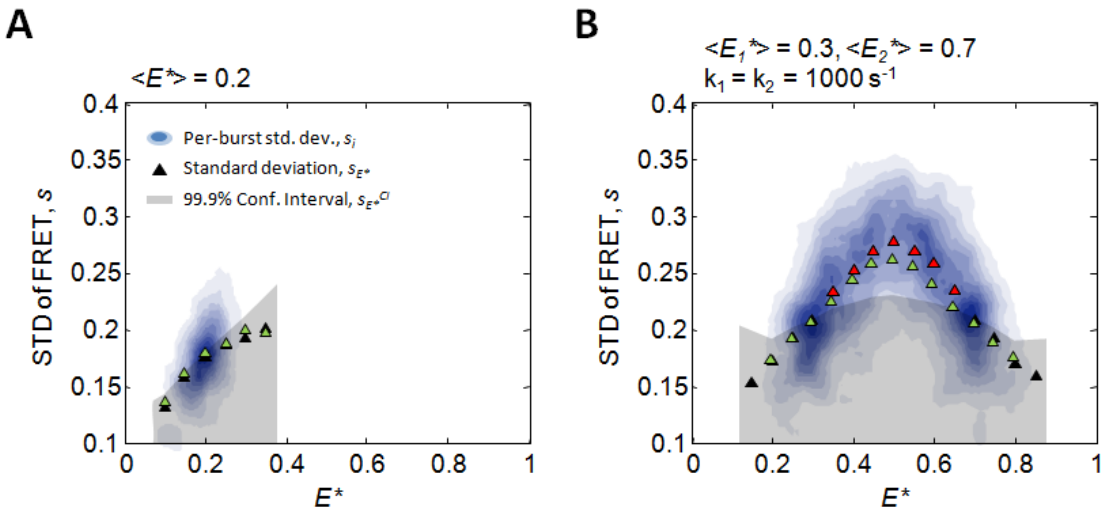

Figure S3. Effect of background on BVA. To illustrate the effects of background on BVA, we first simulated (*A*) a constant-FRET control sample (same as in Fig. S5), and (*B*) a strongly dynamic sample (same as in Fig. 3, *B*). We then repeated these simulations, but added fairly high background (10kHz in the green-excitation green-emission channel, 6kHz in green-excitation red-emission, more than twice that of typical experimental background counts). We performed BVA on the no-background simulations and plotted them, then overlaid the s_{E^*} of the high background simulations (*green triangles*). Whereas the static simulation showed little difference between the s_{E^*} of samples with and without background, the dynamic simulation showed a small but consistent decrease in s_{E^*} at intermediate values of E^*, where dynamics were clearest; this is due to the fact that background, like static species, emits photons in a binomial fashion with respect to the donor and acceptor emission channels, lowering dynamic s_{E^*} values. When using BVA, high background can therefore produce false negatives for dynamics, though it will not generate false positives. We note that background, if high enough to warrant it, can be incorporated into the "Arrival-Time PDA" approach (see Supporting Materials Text).

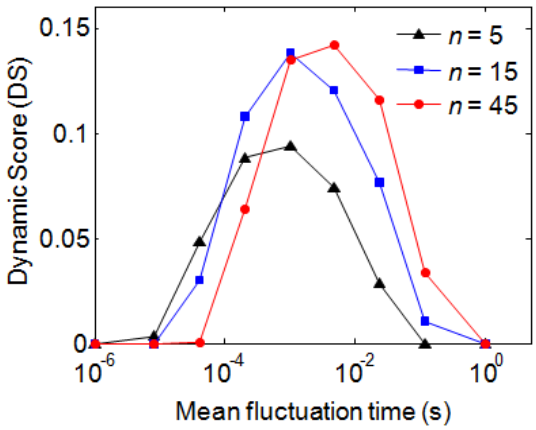

Figure S4. Sensitivity of BVA to dynamics as a function of photon window size, *n*. As in Fig. 3, *D* and *E*, we plotted the Dynamic Score (DS) for a series of simulated two-state dynamic species with different fluctuation timescales, while varying the photon window size, *n*, used to perform BVA. DS is a least-squares-like measure of the difference between the expected (σ_{E^*}) and observed (s_{E^*}) standard deviations over all values of E^* for which dynamics are significant, Eq. 9, such that all nonzero points indicate significant evidence for dynamics, and the larger the DS, the greater the evidence for dynamics. We found that increasing the photon window size has two effects: it increases the DS around the diffusion timescale, and slightly translates the DS plot to slower timescales. This translation results in detection of slow dynamics that were not previously detectable (~10^{-1} s timescale), but failure to identify faster dynamics (~10^{-5} s) that had been detected at the smaller window size. As a result, no photon window is optimal for detecting dynamics on all timescales, but faster or slower dynamics may be more easily detected with smaller or larger photon windows, respectively. Altering photon window size may therefore be useful for extending the range of detectable dynamic timescales with BVA.

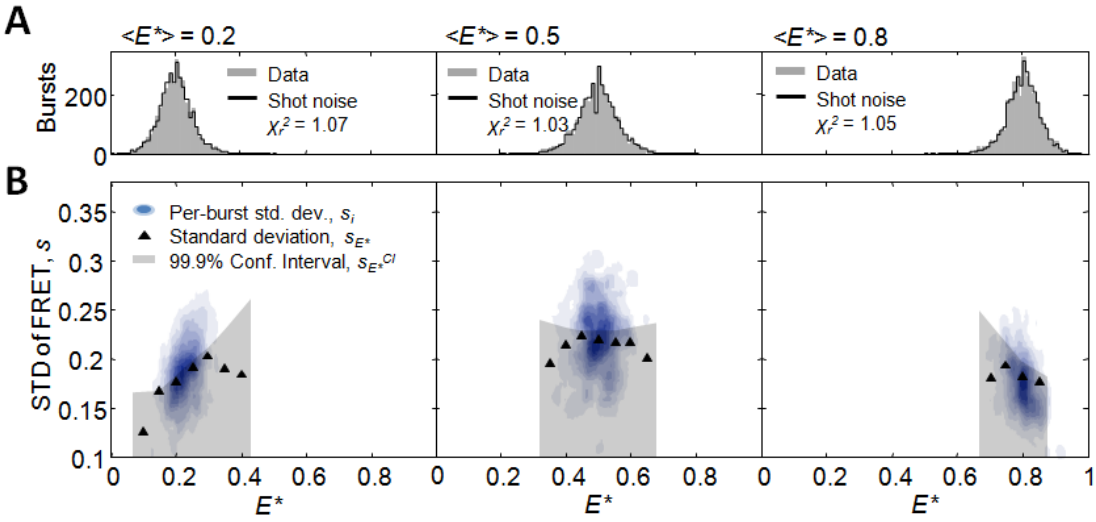

Figure S5. Simulations show good agreement between s_{E^*} and confidence intervals for simulated static FRET species. Simulations were carried out for FRET pairs with $\langle E^* \rangle$ values of either 0.2, 0.5 or 0.8. (A) Photon Distribution Analysis (PDA) was used to confirm that simulated data exhibits no broadening beyond the predicted shot-noise limited histogram for each value of $\langle E^* \rangle$ ($\chi_r^2 \approx 1$ in all cases). (B) These data were subsequently analyzed by BVA, using a photon window size of *n=5*. In all cases, s_{E^*} values (triangles) fall below the strict, 99.9% one-tail confidence interval (gray region), as expected for static FRET species.

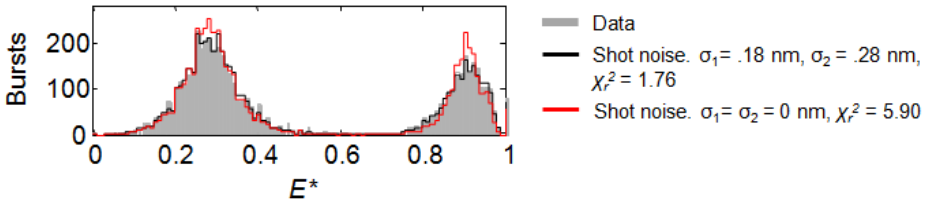

Figure S6. Static hairpin controls show broadening beyond shot noise. We analyzed a mixture of open and closed static control hairpins with smFRET and fit the distributions with PDA (same data as in Fig. 4, *B*). Whereas the distributions could be fit by assuming a Gaussian distribution of originating FRET values (*black line*; $\langle E_{open}^{*} \rangle = 0.285 \pm 0.002$, $\sigma^{r}_{open} = 0.18 \pm 0.01$ nm, $\langle E_{closed}^{*} \rangle = 0.905 \pm 0.001$ and $\sigma^{r}_{closed} = 0.28 \pm 0.02$ nm; $\chi^{2}_{r} = 1.76$), shot noise alone could not account for the widths of each distribution (*red line*; $\langle E_{open}^{*} \rangle = 0.285$, $\langle E_{closed}^{*} \rangle = 0.905$, $\chi^{2}_{r} = 5.90$).

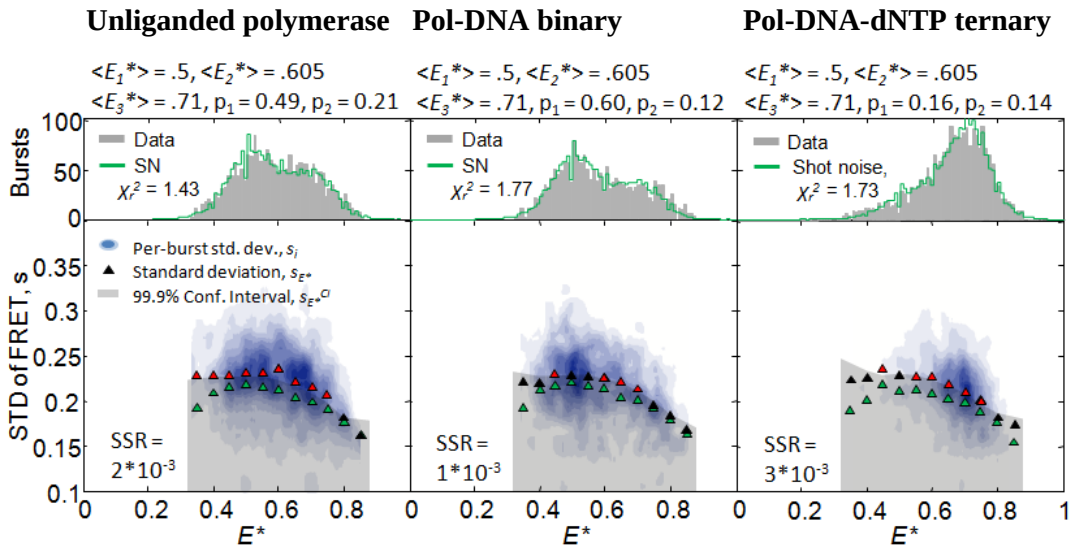

Figure S7. Static three-species models cannot account for DNA Pol I dynamics. As an alternative to the two-species static predictions in Fig. 5, in which we fit for the standard deviation of each of two species, we tested whether a three-species static model, where all widths are fixed ($\sigma^r = 0.18$ nm) but relative concentrations of each species are allowed to vary, could account for the data in the (*left*) unliganded polymerase, (*center*) Pol-DNA binary complex or (*right*) ternary complex. We first used PDA to achieve a fit to the E^* histograms (*top panels*); we held the FRET of the fingers-open and fingers-closed states fixed ($\langle E_1^* \rangle = 0.5$, $\langle E_3^* \rangle = 0.71$) while adding an intermediate state ($\langle E_2^* \rangle = 0.605$), and fitting using two parameters to describe the frequencies of the first two species (p_1 and p_2; the frequency of the third species, p_3, is simply: $1 - p_1 - p_2$). While in all cases the three-species fit provided a satisfactory match to the E^* histogram ($\chi_r^2 < 2$), BVA plots (*bottom panels*) showed that the s_{E^*} for the static predictions (*green triangles*) deviate strongly from the s_{E^*} observed for the data (*black and red triangles*). Indeed, the measured sum of squared residuals, *SSR*, between each set of data and its predicted s_{E^*} was similar to that of the static two-state predictions in Fig. 5, being about an order of magnitude larger than the dynamic model predictions for the same data.

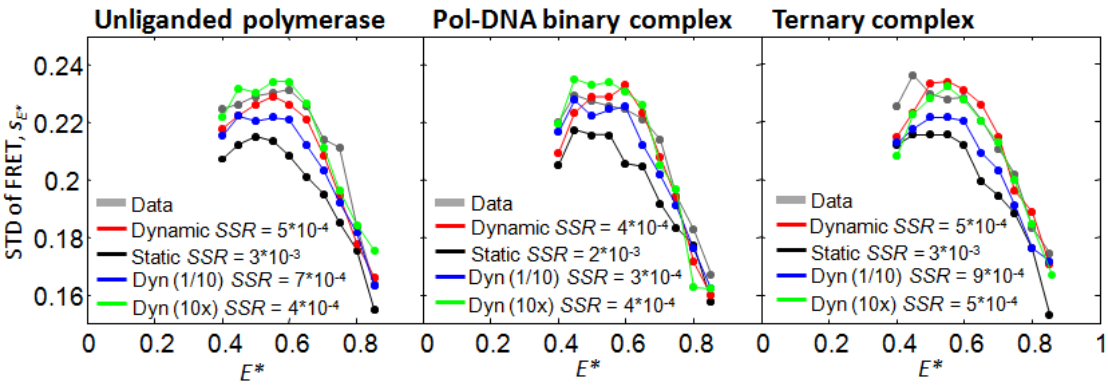

Figure S8. The dynamic model of *E heterogeneity in the Klenow Fragment is robust to fluctuation timescale.** We repeated our BVA analysis of the unliganded Klenow Fragment (*left*), Pol-DNA binary complex (*middle*) or Pol-DNA-dNTP ternary complex (*right*), from Fig. 5. In addition to analyzing experimental data (*grey*) and best-fit dynamic (*red circles*) and static (*black circles*) PDA predictions with BVA, we also analyzed dynamic predictions where both the forward and backward rate constants, k_{open} and k_{close}, had been increased (*green circles*) or decreased (*blue circles*) by ten-fold. In all cases, the dynamic predictions achieved a lower SSR with respect to the experimental data, than did the static prediction.

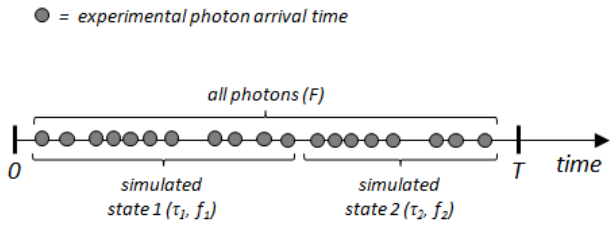

Figure S9. Schematic diagram of arrival-time dynamic PDA method. A single burst is shown above, beginning at time 0 and ending at time *T*, with *F* photons (arrival times indicated with *grey circles*). To implement either the original, or arrival-time, dynamic PDA method, we first simulate kinetic switching among states; for the burst shown, the molecule switches stochastically from state 1 to state 2 about half-way through the burst. In the original dynamic PDA method, the total times spent in each state, τ_1 and τ_2, were recorded; assuming a uniform intensity distribution, the distribution of photons in each state, $P(\vec{f})$, is simply a multinomial with the time spent in each state, Eq. S6. In the updated "Arrival-Time" dynamic PDA method, however, we directly measure the number of experimental photon arrival times falling in each simulated state, f_1 and f_2. Unlike the original PDA method, this approach effectively draws from the arrival time distribution to calculate $P(\vec{f})$, incorporating details about the illumination geometry that are lost under the uniform-intensity assumption. As a result, this method produces more accurate PDA predictions for diffusing dynamic species (Fig. S2), while preserving arrival-time information for analysis with BVA.

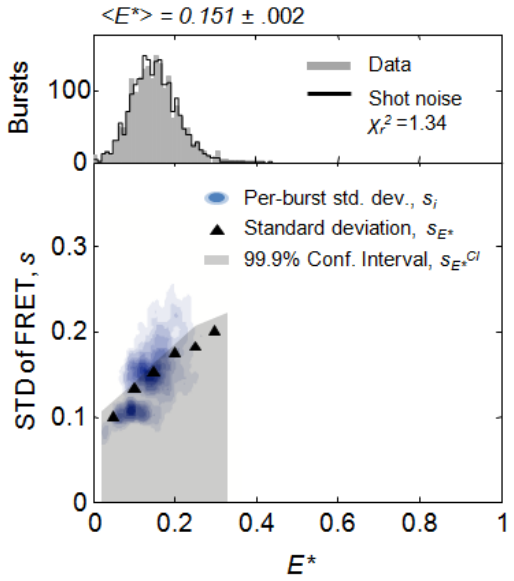

Figure S10. PDA and BVA analysis of an experimental donor-only FRET control. This control is a double-stranded DNA labeled with only the donor fluorophore (Fig. S1, *A*), such that the apparent proximity ratio is due only to spectral leakage of donor emission into the acceptor detection channel. PDA shows a shot noise-limited E^* distribution ($\langle E^* \rangle = 0.15 \pm .0018$, $\chi_r^2 = 1.34$; *top panel*), while BVA shows consistency of the observed s_{E^*} with a static underlying FRET value, as expected (*bottom panel*).

Supporting References:

1. Fries, J. R., L. Brand, C. Eggeling, M. Kollner, and C. A. M. Seidel. 1998. Quantitative identification of different single molecules by selective time-resolved confocal fluorescence spectroscopy. *J. Phys. Chem. A* 102:6601-6613.
2. Antonik, M., S. Felekyan, A. Gaiduk, and C. A. M. Seidel. 2006. Separating structural heterogeneities from stochastic variations in fluorescence resonance energy transfer distributions via photon distribution analysis. *J. Phys. Chem. B* 110:6970-6978.
3. Kalinin, S., S. Felekyan, A. Valeri, and C. A. M. Seidel. 2008. Characterizing multiple molecular states in single-molecule multiparameter fluorescence detection by probability distribution analysis. *J. Phys. Chem. B* 112:8361-8374.
4. Kalinin, S., S. Felekyan, M. Antonik, and C. A. M. Seidel. 2007. Probability distribution analysis of single-molecule fluorescence anisotropy and resonance energy transfer. *J. Phys. Chem. B* 111:10253-10262.
5. Watkins, L. P., H. Y. Chang, and H. Yang. 2006. Quantitative single-molecule conformational distributions: A case study with poly-(L-proline). *J. Phys. Chem. A* 110:5191-5203.
6. Santoso, Y., J. P. Torella, and A. N. Kapanidis. 2010. Characterizing Single-Molecule FRET Dynamics with Probability Distribution Analysis. *Chemphyschem* 11:2209-2219.
7. Gopich, I. V., and A. Szabo. 2009. Decoding the Pattern of Photon Colors in Single-Molecule FRET. *J. Phys. Chem. B* 113:10965-10973.
8. Kenney, J. F., and E. S. Keeping. 1951. The Distribution of the Standard Deviation. In Mathematics of Statistics, Pt. 2, 2nd ed. Van Nostrand, Princeton, NJ. 170-173.
9. Abidi, H. 2007. Bonferroni and Sidak corrections for multiple comparisons. In Encyclopedia of Measurement and Statistics. Sage, Thousand Oaks (CA). 103-107.
10. Nir, E., X. Michalet, K. M. Hamadani, T. A. Laurence, D. Neuhauser, Y. Kovchegov, and S. Weiss. 2006. Shot-noise limited single-molecule FRET histograms: Comparison between theory and experiments. *J. Phys. Chem. B* 110:22103-22124.
11. Lee, N. K., A. N. Kapanidis, Y. Wang, X. Michalet, J. Mukhopadhyay, R. H. Ebright, and S. Weiss. 2005. Accurate FRET measurements within single diffusing biomolecules using alternating-laser excitation. *Biophys. J.* 88:2939-2953.